Motor Unit Identification From High-Density Surface Electromyograms in Repeated Dynamic Muscle Contractions

Vojko Glaser and Aleš Holobar, *Member, IEEE*

***Abstract*— We describe the method for identification of motor unit (MU) firings from high-density surface electromyograms (hdEMG), recorded during repeated dynamic muscle contractions. A new convolutive data model for dynamic hdEMG is presented, along with the pulse-to-noise ratio (PNR) metric for assessment of MU identification accuracy and analysis of the impact of MU action potential (MUAP) changes in dynamic muscle contractions on MU identification. We tested the presented methodology on signals from biceps brachii, vastus lateralis, and rectus famoris muscles, all during different speeds of dynamic contractions. In synthetic signals with excitation levels of 10%, 30% and 50%, and MUAPs experimentally recorded from biceps brachii muscle, the presented method identified 15 ± 1, 18 ± 1, and 20 ± 1 MUs per contraction, respectively, all with average sensitivity and precision >90% and PNR >30 dB. In experimental signals acquired during low force contractions of vastus lateralis and rectus femoris muscle, the method identified 9.4 ± 1.9 and 7.8 ± 1.4 MUs with PNR values of 35.4 ± 3.6 and 34.1 ± 2.7 dB. In comparison with the previously introduced Convolution Kernel Compensation method, the capability of the new method to follow dynamic MUAP changes is confirmed, also in relatively fast muscle contractions.**

***Index Terms*— Motor unit, firing pattern, high-density electromyogram, dynamic contraction, decomposition, motor unit action potential.**

I. Introduction

SKELETAL muscles spatially spread and amplify the neural codes that control human movements [5], [6], [17] and have been under intense investigation in the fields of neurophysiology, neurology, rehabilitation, prosthetics, ergonomics and many others [22]. Information on motor units activity has also contributed to better understanding of many pathologies such as stroke [20] and pathological tremor [8], [9], [16], [29] and basic neurophysiologic research of reflexes [32] and aging [31], among the others. Indeed, in many different healthy and pathological conditions the neuromuscular junctions remain stable, thus, the activity of individual motor units (MUs) reflects the neural codes sent down the motor neurons [5], [6], [17].

Recently, different methodologies for acquisition, assessment and interpretation of large number of neural codes via MU firing pattern identification have been introduced [5], [6], [26], [27], complementing the indwelling electromyography (EMG) with analysis of population coding in relatively large pools of MUs. Both surface and indwelling multichannel recording system have been introduced [1], [22], [24], [27], [30]. They both acquire activities of several tens of MUs, superimposed into interferential EMG patterns. Therefore, different computer-aided techniques have been proposed for extraction of the individual MU firing patterns from acquired multichannel EMG signals [2], [3], [5], [6], [12]–[17], [19], [25], [27], [28]. Due to the complexity of the EMG mixing process, which is typically modelled by convolutive multiple-input-multiple-output system [12]–[15], identification of individual MU firing pattern has been largely limited to isometric muscle contractions, in which the geometry of the muscle and surrounding tissue does not change considerably. In such conditions, the MU action potentials (MUAPs), acquired by the uptake electrodes are relatively stationary and the main EMG nonstationarity comes from the MU recruitment and firing rates modulation. The isometric muscle contractions are then used as a test bench for the functional evaluation of neural system. Whether or not the population coding of MUs in isometric conditions is representative also for the dynamic conditions remains an open research question.

In dynamic contractions, the muscle shortening affects the latency at which the action potential terminates at the muscle-tendon junction, causing the nonpropagating MUAP component. Also, the distances between the muscle fibers and the uptake electrodes change with muscle shortening. Both factors affect the detected MUAP shapes [22]. Namely, interposed tissue acts as a low-pass filter that suppresses high frequencies. The intensity of this filtering is related to the interposed tissue thickness and varies substantially with muscle shortening.

Manuscript received August 9, 2018; revised October 29, 2018, November 20, 2018 and November 27, 2018; accepted December 2, 2018. Date of publication December 17, 2018; date of current version January 9, 2019. This work was supported in part by the Slovenian Research Agency under Project J2-7357 - Exact quantification of muscle control strategies and co-activation patterns in robot-assisted rehabilitation of hemiparetic patients and Programme funding P2-0041. *(Corresponding author: Aleš Holobar.)*

The authors are with the Faculty of Electrical Engineering and Computer Science, University of Maribor, 2000 Maribor, Slovenia (e-mail: vojko.glaser@um.si; ales.holobar@um.si).

Digital Object Identifier 10.1109/TNSRE.2018.2885283

This volume conductor changes are reflected in the acquired EMG, but are not related to the changes of the muscle excitation during the human motion. Therefore, both aforementioned factors of EMG nonstationarity need to be separated when we interpret EMG.

In this study, we extend the previously introduced Convolution Kernel Compensation (CKC) method for EMG decomposition [12]–[15] from isometric to repeated dynamic muscle contractions. Moreover, we show that the extent of MUAP changes in dynamic contractions is not only muscle and contraction, but also MU specific. We therefore introduce a MU specific measure of MUAP changes that can be used directly in the space of identified MU spike trains and does not depend on any external measure of muscle geometry or joint angle. This greatly simplifies the acquisition of dynamic EMG signals. We test the newly proposed methodology for dynamic EMG decomposition on a set of high-density surface EMG (hdEMG) signals from biceps brachii, vastus lateralis and rectus femoris muscle of young healthy subjects and show that Pulse-to-Noise Ratio [17], previously introduced for measuring the accuracy of MU identification in isometric muscle contractions, can also be applied to dynamic conditions.

II. Methods

A. hdEMG Modelling in Dynamic Muscle Contractions

In dynamic muscle contractions, we model multichannel surface EMG by the the convolutive data model [12], [13]:

$$\mathbf{y}(n) = \mathbf{H}(n)\bar{\mathbf{t}}(n) + \boldsymbol{\omega}(n), \tag{1}$$

where $\boldsymbol{y}(n) = [y_1(n) \dots y_M(n)]^T$ combines the n-th sample of M hdEMG measurements, $\boldsymbol{\omega}(n) = [\omega_1(n) \dots \omega_M(n)]^T$ is noise vector and $\bar{\mathbf{t}}(n) = [t_1(n), t_1(n-1) \dots t_1(n-L) \dots t_M(n) \dots t_M(n-L)]^T$ contains $L+1$ samples of the MU spike trains [12], [13]. The j-th MU spike train is defined as:

$$t_{\mathrm{j}}(\mathrm{n}) = \sum\nolimits_{\mathrm{k}} \delta\left(n - \tau_{\mathrm{j}}(k)\right), \quad j = 1 \dots N, \tag{2}$$

whereat δ is the unit-sample pulse and the k-th MUAP of the j-th MU appears at time $\tau_j(k)$.

The mixing matrix $\mathbf{H}(n) = [\mathbf{H}_1(n) \dots \mathbf{H}_N(n)]$ comprises all the $L+1$ samples long MUAPs as detected by the surface electrodes, where

$$\mathbf{H}_{\mathrm{j}}(n) = \begin{bmatrix} h_{1\mathrm{j}}(n,0) & \dots & h_{1\mathrm{j}}(n,L) \\ \vdots & \ddots & \vdots \\ h_{\mathrm{Mj}}(n,0) & \dots & h_{\mathrm{Mj}}(n,L) \end{bmatrix}, \quad j = 1 \dots N. \tag{3}$$

and $h_{\mathrm{ij}}(n,l)$ stands for the l-th sample of the j-th MU's action potential as detected by the i-th uptake electrode at the time of the n-th EMG sample.

In isometric non-fatiguing muscle contractions, the mixing matrix $\mathbf{H}(n)$ may be assumed stationary. In such a case, classical hdEMG decomposition techniques, such as CKC, can be applied to the entire hdEMG signal [12]–[15], [21]. In slow dynamic muscle contractions and long isometric contractions, MUAP shapes change gradually, either due to geometric deformations or due to muscle fatigue [22]. Therefore, the hdEMG needs to be divided into short enough epochs in which the $\mathbf{H}(n)$ does not change significantly. Consequently classic hdEMG decomposition techniques need to be applied independently to each signal epoch. In a typical setup, signal epochs overlap for 50% in order to support efficient merging of different fragments of the MU spike train, identified from different hdEMG epochs.

In moderate and fast dynamic contractions, $\mathbf{H}(n)$ becomes nonstationary, but still follows the locality principle in a sense that it changes gradually and these changes can be modeled by continuous function. Therefore, we may rewrite the model (1) as:

$$\begin{aligned} \mathbf{y}(n) &= \bar{\mathbf{H}}\bar{\mathbf{t}}(n) + \Delta\mathbf{H}(n)\bar{\mathbf{t}}(n) + \boldsymbol{\omega}(n) \\ &= \bar{\mathbf{H}}\bar{\mathbf{t}}(n) + \mathbf{z}(n) + \boldsymbol{\omega}(n), \end{aligned} \tag{4}$$

where $\bar{\mathbf{H}}$ is the average $\mathbf{H}(n)$ over the observed time interval and $\Delta\mathbf{H}(n)$ models the differences between the $\bar{\mathbf{H}}$ and the true mixing matrix $\mathbf{H}(n)$. From the isometric hdEMG decomposition viewpoint [14]–[16], we may consider $\mathbf{z}(n) = \Delta\mathbf{H}(n)\bar{\mathbf{t}}(n)$ in (4) a model error that adds to the noise term $\boldsymbol{\omega}(n)$ in MU identification.

In repeated non-fatiguing muscle contractions $\mathbf{H}(n)$ and $\Delta\mathbf{H}(n)$ become cyclostationary. $\mathbf{z}(n)$ is not necessarily strictly cyclostationary as it also depends on the firing times $\bar{\mathbf{t}}(n)$. Nevertheless, as demonstrated by the results in Section IV, cyclostationarity is at least partially reflected in correlation matrix of $\mathbf{z}(n)$. We can assume $\mathbf{z}(n)$ to be zero-mean.

B. Initial MU Spike Estimation in Dynamic Contractions

In isometric contractions, the CKC estimates the j-th MU's spike train as [12], [13]:

$$\hat{t}_j(n) = \mathbf{c}_{\mathrm{t_j y}}^{\mathrm{T}} \mathbf{C}_{\mathbf{y}}^{-1} \mathbf{y}(n), \tag{5}$$

where $\mathbf{C}_{\mathbf{y}} = E\left(\mathbf{y}(n)\mathbf{y}^T(n)\right)$ is correlation matrix of hdEMG measurements, $\mathbf{c}_{t_j\mathbf{y}} = E\left(t_j(n)\mathbf{y}(n)\right)$ is the cross-correlation vector between $t_j(n)$ and $\mathbf{y}(n)$ and $E(.)$ stands for mathematical expectation. Note that $\mathbf{c}_{t_j\mathbf{y}}$ is not known in advance but can be estimated by gradient optimization described in [14] and [17].

The mean square error between the true and CKC-estimated spike train of the j-th MU can be modelled by [18]

$$E\left(\left(t_j(n) - \hat{t}_j(n)\right)^2\right) = \mathbf{B}_{\mathrm{jj}}(n) \tag{6}$$

where $\mathbf{B}_{\mathrm{jj}}(n)$ denotes the j-th diagonal element of $\mathbf{B}(n) = \mathbf{C_t} - \mathbf{C_t}\bar{\mathbf{H}}^{\mathrm{T}}\left(\boldsymbol{\Theta}(n) + \bar{\mathbf{H}}\mathbf{C_t}\bar{\mathbf{H}}^{\mathrm{T}}\right)^{-1}\bar{\mathbf{H}}\mathbf{C_t}$ and $\mathbf{C_t} = E\left(\mathbf{t}(n)\mathbf{t}^T(n)\right)$ stands for correlation matrix of motor unit spike trains. In isometric conditions, $\boldsymbol{\Theta}(n)$ is correlation matrix of noise $\boldsymbol{\omega}(n)$, whereas in dynamic conditions, $\boldsymbol{\Theta}(n)$ is correlation matrix of model errors and noise $\boldsymbol{\psi}(n) = \mathbf{z}(n) + \boldsymbol{\omega}(n)$. Then, by following the derivations in [18], we can redefine the Pulse-to-Noise Ratio (PNR) of $\hat{t}_{\mathrm{j}}(n)$ as:

$$\begin{aligned} PNR\left(\hat{t}_{\mathrm{j}}(n)\right) &= 10 \cdot \log\left(\frac{E\left(\hat{t}_j^2(n)\Big|_{\hat{t}_{\mathrm{j}}(n)=1}\right)}{E\left(\hat{t}_j^2(n)\Big|_{\hat{t}_{\mathrm{j}}(n)=0}\right)}\right) \\ &= 10 \cdot \log\left(1 + \frac{c_{t_{\mathrm{j}}t_{\mathrm{j}}} - \mathbf{B}_{\mathrm{jj}}(n)}{c_{t_{\mathrm{j}}t_{\mathrm{j}}}\mathbf{B}_{\mathrm{jj}}(n)}\right) \end{aligned} \tag{7}$$

where $c_{t_j t_j}$ is the j-th diagonal element of $\mathbf{C_t}$. Note that PNR $\to \infty$ when $\mathbf{\Theta}(n) \to 0$, and PNR $\to 0$ when $\mathbf{\Theta}(n) \to \infty$.

Let us now use Eq. (5) to identify the $\hat{t}_j(n_a)$ on the interval $n_a \in [a_1, a_2]$ and compute the $\mathbf{c}_{t_j \mathbf{y}}$ on this interval:

$$\mathbf{c}_{t_j \mathbf{y}, n_a} = \sum_{n_a \in [a_1, a_2]} t_j(n_a)\, \mathbf{y}(n_a) \tag{8}$$

Then, we rewrite Eq. (5) to

$$\hat{t}_{j,n_a}(n) = \mathbf{c}^{\mathbf{T}}_{t_j \mathbf{y}, n_a} \left(\sum_{\substack{p \in [a_1, a_2] \\ \cup [b_1, b_2]}} \mathbf{y}(p)\, \mathbf{y}^T(p) \right)^{-1} \mathbf{y}(n) \tag{9}$$

where $[a_1, a_2]$ and $[b_1, b_2]$ are two non-overlapping time intervals and $n \in [a_1, a_2] \cup [b_1, b_2]$. Let us further assume that the interval $[a_1, a_2]$ is short enough so that $\Delta\mathbf{H}(n_a)$ and $\mathbf{\Theta}(n_a)$ do not change considerably for $n_a \in [a_1, a_2]$. Then, $PNR(n_a)$ is approximately constant on this interval, whereas, according to Eq. (7), its value on the interval $n_b \in [b_1, b_2]$ depends on $\Delta\mathbf{H}(n_b)$. The larger the difference $\Delta\mathbf{H}(n_a) - \Delta\mathbf{H}(n_b)$, the lower the PNR$(n_b)$. This is, in fact, imposed by limiting the calculation of $\mathbf{c}_{t_j \mathbf{y}}$ in Eq. (8) to the time interval $[a_1, a_2]$. Therefore, we may use the PNR metric in Eq. (7) to search for the time intervals $[b_1, b_2]$ on which the $\mathbf{H}(n_b) \approx \mathbf{H}(n_a)$ and then improve the estimate of $\mathbf{c}_{t_j \mathbf{y}}$ and $\hat{t}_j(n)$ by recalculating them over all time intervals with similar mixing matrices $\mathbf{H}(n)$. This is crucial for reducing the impact of noise and model errors in $\mathbf{c}_{t_j \mathbf{y}}$ estimation [18].

In the sequel, we will refer to PNR metric, calculated on the shorter time intervals as local PNR, whereas the PNR metric, calculated over the whole time range of hdEMG signals will be referred to as global PNR.

As indicated by Eq. (7) and further demonstrated in Fig. 3, the changes in the local PNR are MU specific. Namely, the PNR value in Eq. (7) depends on the shape of the j-th MU's MUAPs in all the hdEMG channels [18]. Thus, local PNR allows for MU specific selection of time intervals with relatively constant $\mathbf{c}_{t_j \mathbf{y}}$ and $\mathbf{C}_{\mathbf{y}}$. Furthermore, similar to $\mathbf{H}(n)$, the local PNR follows the locality principle and gradually decreases its value with the increase of difference between the $\mathbf{H}(n_a)$ and $\mathbf{H}(n_b)$ in Eqs. (8) and (9).

C. MU Tracking in Dynamic Muscle Contractions

The procedure introduced in the previous section allows us to estimate the MU spike train $\hat{t}_{j,n_a}(n)$ on all the intervals $n_b \in [b_1, b_2]$ where the mixing matrix $\mathbf{H}(n_b)$ is similar to the initial matrix $\mathbf{H}(n_a)$. For identification of spikes outside these intervals, we need to update $\mathbf{c}_{t_j \mathbf{y}}$ and shift it towards new intervals while reliably tracking the spikes of the selected MU. For this reason, we update the $\mathbf{c}_{t_j \mathbf{y}}$ vector in (8) as:

$$\hat{c}_{t_j, \mathbf{y}}(n_a) = \sum_{n \in [a_1, a_2]} f\left(t_{j,n_a}, n\right) \mathbf{y}(n) \tag{10}$$

Here $f(.)$ denotes the window function. As demonstrated in Fig. 4, $f(.)$ may be used to increase the MU spikes at selected portion of the $[a_1, a_2]$ interval. For example, function $f(.)$ that is depicted in the upper panel of Fig. 4 increases the estimated MU spikes at the beginning of the interval $[a_1, a_2]$, left-shifting the $\hat{\mathbf{c}}_{t_j, \mathbf{y}}(n_a)$ in (10) by making it similar to the $\mathbf{c}_{t_j \mathbf{y}}\left(n_{a-\Delta a/2}\right)$. On the other hand, the $f(.)$ function that is depicted in the lower panel of Fig. 4 increases the spikes at the end of the interval $[a_1, a_2]$, shifting $\hat{\mathbf{c}}_{t_j, \mathbf{y}}(n_a)$ to the right, i.e., towards $\mathbf{c}_{t_j \mathbf{y}}\left(n_{a+\Delta a/2}\right)$. By wisely selecting $f(.)$ and gradually moving the $[a_1, a_2]$ interval in (10) across the entire signal, different portions of MU spike train are identified (Pseudocode 1).

Pseudocode 1 The Proposed Cyclostationary CKC Method

1:	Select the interval $[a_1, a_2]$ and step Δa. Initialize j=1.
2:	Initialize $\Upsilon = \emptyset$ to empty set and let $t_j(n) = \mathbf{0}$
3:	Use classical CKC [12] to estimate $\hat{t}_j(n_a)$ for $n_a \in [a_1, a_2]$.
4:	Use Eq. (8) to compute $\mathrm{c}_{t_j y, n_a}$ on $[a_1, a_2]$.
5:	Set $b_1 = 0$ and $\mathbf{c}_{t_j y} = \mathbf{0}$
6:	While $b_1 + \Delta a <$ signal length Use Eq. (9) to compute $\hat{t}_{j,n_a}(n)$, for $n \in [a_1, a_2] \cup [b_1, b_1 + \Delta a]$. Segment $\hat{t}_{j,n_a}(n)$ into spikes and base-line noise [18] and use Eq. (7) to calculate $PNR\left(\hat{t}_{j,n_a}(n_b)\right)$ where $n_b \in [b_1, b_1 + \Delta a]$. If $PNR\left(\hat{t}_{j,n_a}(n)\right) \geq 28$ dB $\mathbf{c}_{t_j y} = \mathbf{c}_{t_j y} + \sum_{n \in [b_1, b_1 + \Delta a]} \hat{t}_{j,n_a}(n)\, \mathbf{y}(n)$ $\Upsilon = \Upsilon \cup [b_1, b_1 + \Delta a]$ $b_1 = b_1 + \Delta a$
7:	Normalize $\mathbf{c}_{t_j y}$ so that $\mathbf{c}_{t_j y} = \mathbf{c}_{t_j y} / \left\|\mathbf{c}_{t_j y}\right\|$ and use it in Eq. (5) to estimate $\hat{t}_j(n)$ on the entire signal length.
8:	Add current spike train estimate to the previous ones: $t_j(n) = t_j(n) + \hat{t}_j(n)$
9:	Search for sample c in Υ such that $c+1$ is not in Υ. If found Use Eq. (10) with $f\left(\hat{t}_j(n), n\right) = \hat{t}_j(n) \cdot (0.5 - (c - \Delta a - n)/\Delta a)$ to estimate new "right-shifted" $\hat{c}_{t_j, y}(n_c)$ on $n_c \in [c - \Delta a, c]$. Update $\mathrm{c}_{t_j y, n_a} = \hat{c}_{t_j, y}(n_c)$ and set $\Upsilon = \Upsilon \cup [c + 1, c + \Delta a/2]$ and $[a_1, a_2] = [c - \Delta a/2, c + \Delta a/2]$. Go to step 5.
10:	Search for sample c in Υsuch that $c-1$ is not in Υ. If found Use Eq. (10) with $f\left(\hat{t}_j(n), n\right) = \hat{t}_j(n) \cdot (0.5 + (c + \Delta a - n)/\Delta a)$ to estimate new "left-shifted" $\hat{c}_{t_j, y}(n_c)$ on $n_c \in [c, c + \Delta a]$. Update $\mathrm{c}_{t_j y, n_a} = \hat{c}_{t_j, y}(n_c)$ and set $\Upsilon = \Upsilon \cup [c - \Delta a/2, c - 1]$ and $[a_1, a_2] = [c - \Delta a/2, c + \Delta a/2]$. Go to step 5.
11:	j = j + 1
12:	Repeat steps 2-11 for preselected number of decomposition runs.

The parameter Δa is contraction, muscle and even MU specific (see Fig. 3). We may assess its optimal value by observing the local PNR value, but such a specific optimization may be time consuming. In this study, Δa was fixed to 1/5 of the contraction ramp (see the next section), whereas the number of decomposition runs in step 12 was fixed to 100 [12], [13]. The linearly increasing and decreasing $f(.)$ functions used in Steps 9 and 10 were empirically selected, but we did not extensively test their optimality in different experimental conditions.

III. Experimental Protocol

A. Synthetic Dynamic hdEMG Signals

Validation of dynamic surface EMG decomposition is currently an open research problem. The two source validation approach with simultaneous acquisition and decomposition of surface and indwelling EMG is not feasible in dynamic conditions, whereas the simulators of synthetic dynamic EMG are still under development [10], [23]. In our study, the validation of EMG decomposition was performed by convolving the synthetic MU spike trains with experimentally recorded MUAPs of biceps brachii muscle. For this purpose, slow dynamic contraction of dominant biceps brachii was recorded in five right-handed young males (age of 34.4 ± 5.4 years, height of 1.77 ± 0.05 m and weight of 77.2 ± 5.5 kg). The subjects received a detailed explanation of the study and gave their written informed consent prior to participation. The study was conducted in accordance with Declaration of Helsinki and was approved by the local ethics committee. Array of 13×5 electrodes (OT Bioelettronica, Torino, Italy) with interelectrode distance of 8 mm was centered over the innervation zone of the short head of dominant biceps brachii. The arm was placed in the custom made brace (Fig. 1) with lever rotatable in the sagittal plane. We used adjustable support to fix the elbow joint in the center of the rotation axis. The lever was carefully balanced by mounting the counterweights (Fig. 1). Afterwards, we used wires and custom made pulley system to fix the 1 kg weight on the lever. In this way, the lever acted on the subject's arm with a constant torque of 3 Nm, regardless the elbow joint angle. The subject controlled the brace by hand grip that was adjusted to his forearm length.

Volunteers performed 80 s long slow isokinetic dynamic contraction, starting with elbow fully extended and ending at elbow fully flexed. The brace lever position was tracked by Fastrak motion tracker (Polhemus, USA) and displayed online on the computer monitor, along with the reference lever's position. Monopolar surface EMG signals were sampled at 2048 Hz and 12 bit resolution (EMG-USB2 amplifier, OT Bioelettronica, Torino, Italy), bandpass filtered between 20 and 700 Hz and stored on the computer's hard drive for offline processing.

The recorded signals were divided into 10 s long epoch with 50 % overlapping. Each epoch was independently decomposed by CKC decomposition technique [12], [13] and identified MU spike trains were pairwise compared to identify the MU firing pattern on the entire 80 s of the recorded signals. Identified firing patterns were manually inspected by two experienced operators and all the MUs with irregular firing patterns or with local PNR bellow 30 dB were discarded [18]. In total, 252 different MUs were identified from all the recorded contractions. Their MUAPs were estimated by spike triggered averaging of 36 consecutive 10 s long EMG epochs that overlapped for 7.8 seconds. Finally, MUAPs from all the identified MUs were joined into common MUAP library. Fig. 2 depicts representative example of MUAP shapes at different percentages of muscle shortening and the distribution of their peak-to-peak

Fig. 1. Custom made brace for recording of dynamic hdEMG signals from biceps brachii muscle. The brace lever was rotatable in the sagittal plane and its torque due to the gravity was counterbalanced with counterweights. Before the measurement, additional 1 kg weight was fixed to the brace lever producing a constant torque of 3 Nm to the subject's dominant hand.

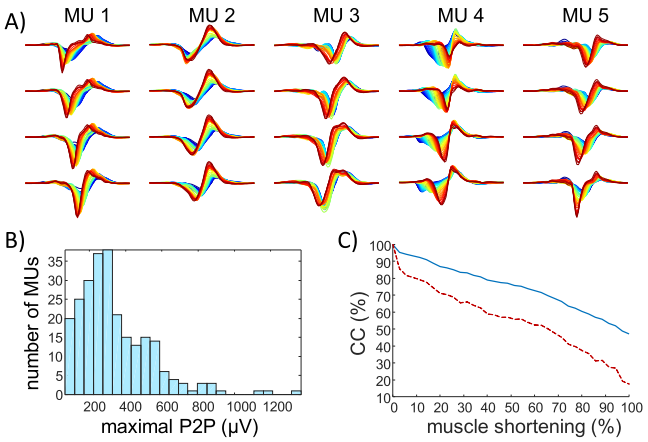

Fig. 2. MUAP changes in dynamic contraction. A) Representative examples of MUAPs from five different MUs, estimated on four neighboring hdEMG channels by spike trigger averaging at 36 different levels of muscle shortening (denoted by different colored lines). Blue and red lines depict the MUAP shape with muscle fully extended and fully shortened, respectively. B) Distribution of maximal peak-to-peak (P2P) amplitude as assessed across all the hdEMG channels and all the muscle shortening levels per motor unit. C) Correlation coefficients between the MUAP shapes at the muscle fully extended and MUAP shapes at different levels of muscle shortening. Blue and red lines depict the mean value and standard deviation, respectively.

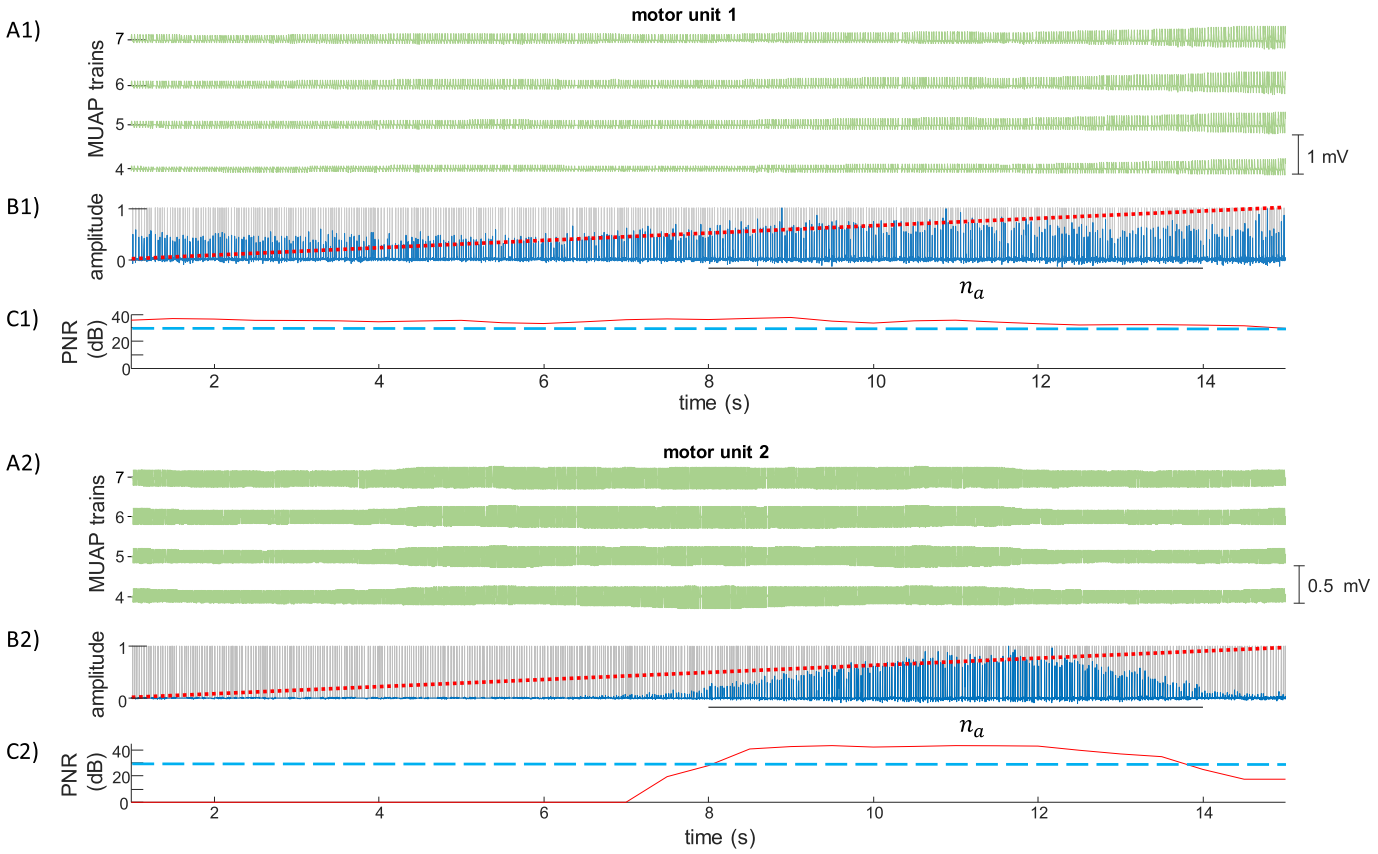

Fig. 3. Simulated MUAP trains in rows 4, 5, 6 and 7 of the central electrode column (panels A1 and A2), simulated (gray) and identified (blue) spike trains (panels B1 and B2) and local PNR values (panels C1 and C2) for two motor units, identified by Eq. (9) from simulated dynamic hdEMG of biceps brachii during the full extension of the elbow joint. The $\mathbf{c}_{t_j \boldsymbol{y}, n_a}$ was calculated on the n_a intervals denoted by the horizontal black lines (panels B1 and B2). The simulated muscle shortening is depicted by red dotted line, whereat the value 1.0 denotes the full muscle shortening. Dashed lines in panels C1 and C2 denote the PNR value of 30 dB.

amplitudes. All the identified MUs extensively changed their MUAPs with muscle shortening (Fig. 2, panels A and C).

MU recruitment and spike trains were generated by the model proposed in [7] with the parameters adapted for the biceps brachii muscle. 200 MUs were simulated and their recruitment followed exponential distribution with many MUs active at low contraction levels and progressively fewer high-threshold MUs [11]. MUs fired at 8 Hz when recruited and linearly increased their firing rate for 0.3 Hz per % of muscle excitation. The MU firing rate peaked at 35 Hz and the last MU was recruited at 80 % of maximal muscle excitation. MU interspike interval variability followed Gaussian distribution with coefficient of variation set to 20%. 60 s long constant 10%, 30% and 50% muscle excitations were simulated, resulting in 105, 155 and 178 active MUs, respectively.

Muscle shortening profiles consisted of full flexion-extension ramps. The number of ramps was set to 2, 3, 6 and 12, resulting in full muscle extension/flexion in 15, 10, 5 and 2.5 s, respectively. The generated spike trains were convolved with dynamic MUAPs from previously described MUAP library, selecting one of the 36 discrete dynamic MUAP shapes (Fig. 2) based on the simulated muscle shortening level.

In each hdEMG decomposition, only the MUs with relatively large MUAPs at the surface of the skin are identified, whereas the other MUs contribute to the physiological noise. Therefore, our library of dynamic MUAPs is biased towards MUs with large MUAPs. In order to compensate for this and generate physiological noise from small and distant MUs, all the MUAPs of each simulated MU were multiplied by a scalar value α before their convolution with MU spikes:

$$\alpha = \frac{e^{\left(\frac{10 \cdot x}{\text{TotNoMUs}}\right)}}{e^{10}} + 0.1, \tag{11}$$

where x is a random integer on the interval [1, TotNoMUs] and TotNoMUs stands for the total number of simulated MUs. This resulted in 10, 15 and 17 MUs with $\alpha > 0.5$ and 13, 19 and 22 MUs with $\alpha > 0.4$, on average, for 10%, 30% and 50% excitation, respectively.

We conducted ten simulation runs for each simulated excitation level and each number of flexion-extension ramps, randomly selecting the scalar factors α in each run. The generated hdEMG signals were sampled at 2048 Hz.

B. Experimental hdEMG

Five healthy young subjects (four males and one female, age of 31.6 ± 4.8 years, height 1.74 ± 0.03 m, weight 70 ± 10 kg) participated to the study that was conducted in accordance with Declaration of Helsinki and was approved by local ethics committee. The subjects received a detailed explanation of the

study and gave their written informed consent prior to participation. hdEMG signals were recorded by two arrays of 13 × 5 electrodes (OT Bioelettronica, Torino, Italy, interelectrode distance of 8 mm) fixed on the surface of the skin above the vastus lateralis and rectus femoris muscle of the dominant leg, respectively, with the five electrode columns approximately aligned with the direction of muscle fibers. The subject was sitting upright on a chair with height adjustable saddle. Both hands rested on the arm holders. In each trail, the subjects performed repetitive flexion-extension movements of the knee, whereat the weight of 1 kg was fixed to the ankle of the dominant leg. The knee joint angle was measured by Fastrak motion tracker (Polheus, USA) and reference knee angle changed at a steady rate from 100 to 160 degrees and back in 10 (moderate speed) and 20 seconds (slow contraction). Here 180 degrees corresponds to full knee extension. The ankle joint was fixed at a 100-degree angle. Each trial consisted of eight (moderate speed) or four (slow speed) consecutive repetitions of the described knee movement, with EMG recorded continuously and knee angle tracked continuously throughout each trial. At least five minutes of rest were provided between trials. All but one subject performed two trials at each speed, whereas subject S1 performed only one trial at each speed.

IV. Results

Fig. 3 depicts the spike trains of two representative MUs, identified by Eq. (9) from synthetic dynamic dhEMG, generated by convolving the experimental MUAPs of biceps brachii muscle with synthetic MU firing patterns at 30 % muscle excitation level. The $\mathbf{c}_{t_j\boldsymbol{y},n_a}$ vector was calculated on the n_a intervals denoted by the horizontal black lines and Eq. (9) was consecutively applied to different n_b intervals. The two MUs demonstrated different sensitivities of identified spike trains to muscle shortening (note the height of MU spikes). The spikes of the first MU were identified over the entire range of muscle contraction, whereas the second MU demonstrated spikes only in the intervals between 50 % and 90 % of muscle shortening. The spike height and, thus, the local PNR followed the locality principle, changing gradually in time. We observed similar behavior of other MUs, regardless the position of n_a interval.

Fig. 4 depicts the effect of different *f(.)* functions in Eq. (10) on the identified MU spike trains. By manipulating *f(.)* we may fine tune the $\mathbf{c}_{t_j\boldsymbol{y}}(n_a)$ vector for identification of spikes in different regions. At the end, the spike trains identified by different *f(.)* functions are summed together to yield the entire spike train (Pseudocode 1).

Fig. 5 depicts the number of MUs, identified by the proposed cyclostationary CKC method from synthetic hdEMG signals, their global PNR values (calculated over the entire time range of hdEMG signals), sensitivity and precision of MU firing identification (identification tolerance was set to 0.5 ms). The results are averaged over ten simulation runs per simulated contraction ramp and excitation level. The number of identified MUs was not dependent on the length of muscle contraction ramp. Also the PNR value, sensitivity and precision did not change considerably with the length of

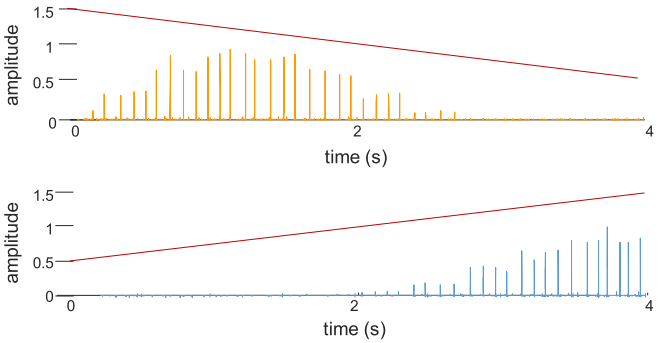

Fig. 4. Impact of different *f(.)* functions on the MU spike train estimation from synthetic dynamic hdEMG. Linearly decreasing *f(.)* function applied to 4 s long interval amplifies MU spikes at the beginning of the interval (upper panel), whereas linearly increasing *f(.)* function amplifies spikes at the end of the interval (lower panel). Depicted *f(.)* functions are defined in Pseudocode 1.

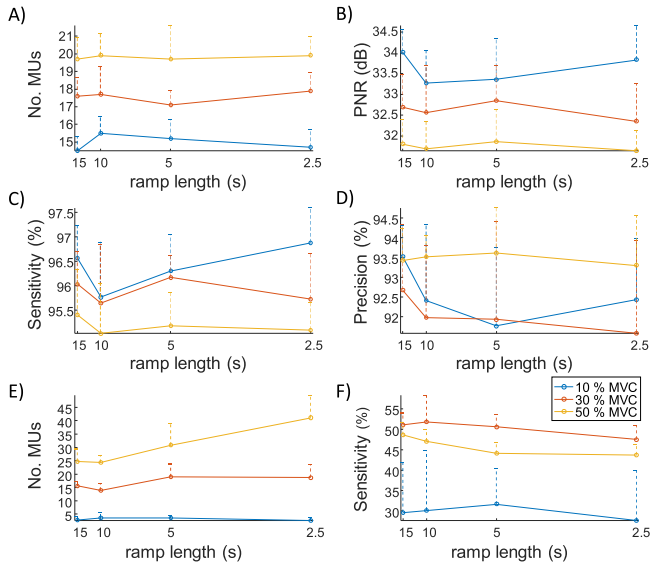

Fig. 5. Results of MU identification from dynamic hdEMG signals with synthetic MU spike trains and experimentally assessed MUAPs from biceps brachii muscle. Panel A depicts the number of MUs (mean ± SD) identified by the proposed cyclostationary CKC as a function of muscle excitation level and speed of muscle contraction. Panels B, C and D depicts their PNR values, sensitivity and precision, respectively. Panels E and F depict the results of decomposition by classic CKC method [12]–[14].

contraction ramp (Fig. 5), demonstrating relative robustness of the presented method to the speed of muscle contraction. In contrast to the proposed cyclostationary CKC, the classical CKC method [14], [18] identified larger number of MUs but with significantly lower sensitivity (Fig. 5). This is in agreement with the examples of identified spike trains in Fig. 3.

Sensitivity and precision of MU firing identification by cyclostationary CKC were positively correlated with the PNR value, whereat all the MUs with the PNR value of 30 dB or greater demonstrated sensitivity ≥90 % and precision ≥90 % (Fig. 6). The false alarm rates were relatively low in all the cases and were negatively correlated with the PNR values (Fig. 6). This is in agreement with the

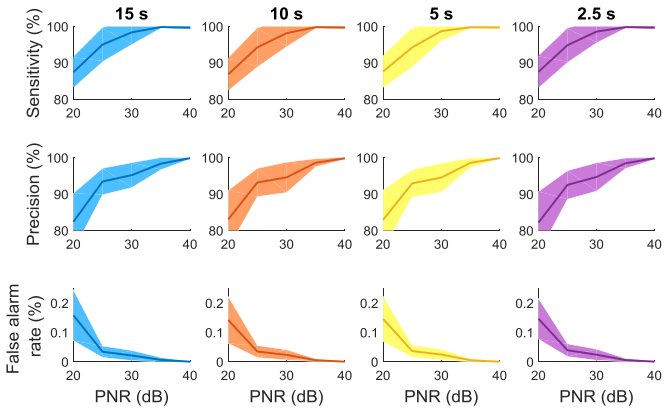

Fig. 6. Sensitivity (mean ± SD), precision (mean ± SD) and false alarm rate (mean ± SD) in identification of MU firings by cyclostationary CKC as a function of PNR and speed of muscle contraction. Results are accumulated across all the simulated muscle excitation levels.

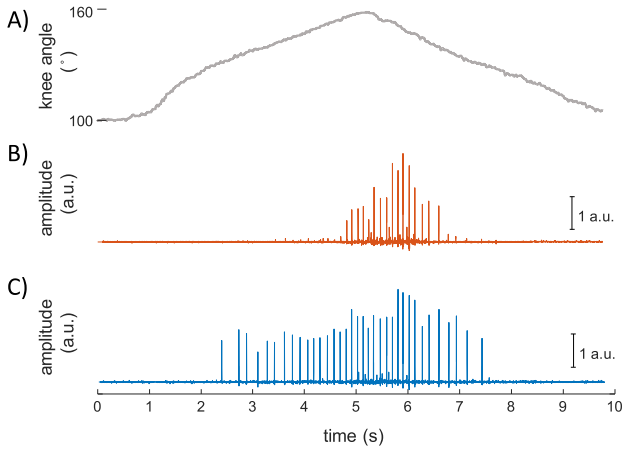

Fig. 7. MU spike trains identified by classic CKC (panel B) and cyclostationary CKC (panel C) during the moderate speed contraction of a vastus lateralis muscle in a representative subject. Panel A depicts the measured knee angle.

results of classical CKC-based MU identification in isometric conditions [18].

Fig. 7 depicts the representative MU spike train identified by cyclostationary CKC (panel C) and classical CKC (panel B) from vastus lateralis muscle. Classical CKC identified only a portion of the MU spike train. These results agree with the ones on synthetic hdEMG signals (Figs. 3 and 5).

Figs. 8 and 9 depict the spike trains and smoothed MU firing rates, identified from experimental hdEMG of vastus lateralis and rectus femoris muscle, respectively, whereas Tables I and II report the results accumulated across all the subjects. On average, 9.4 ± 1.9 and 7.8 ± 1.4 MUs were identified per trail with global PNR > 30 dB from vastus lateralis and rectus femoris muscle, respectively. The number of identified MUs and their PNR values did not depend significantly on the investigated speed of muscle contraction (paired t-test, $p > 0.05$).

V. Discussion

We introduced the new methodology for identification of MU spike trains in dynamic muscle contractions. We also extended previously introduced PNR metric to dynamic conditions and showed that we can use it for assessing the impact of MUAP changes on MU spike trains identified by cyclostationary CKC. Noteworthy, this PNR does not depend on the external measurements of investigated joint angle or any measurement of muscle geometry and can, thus, be used to study hdEMG dynamics in arbitrary and highly complex muscle contractions. Moreover, we showed that the impact of the MUAP changes on identified MU spikes is MU specific.

Theoretically, local PNR value could be used to estimate the optimal Δa parameter in Eq. (10) for each individual MU. However, this would likely add considerably to the computational complexity of MU tracking in dynamic conditions. Therefore, in this study, the local PNR value was used to empirically determine the globally optimal value of Δa parameter, i.e., the same value for all the MUs in each individual speed of muscle contraction. On the other hand, local PNR value was used to determine all the n_b intervals with approximately the same $\mathbf{c}_{t_{jy}}(n_b)$ and, thus, $\mathbf{H}(n_b)$ values. In this way, we significantly increased the robustness of MU spike estimation to model errors in (4).

The results on the synthetic EMG signals with modelled MU spike trains and experimentally recorded MUAPs demonstrated relatively strong robustness of the proposed methodology to the speed of muscle contraction. Neither the number of identified MUs nor their PNR values changed considerably when the speed of muscle contraction was increased,

TABLE I
Number and PNR of MUs Identified From Vastus Lateralis Muscle

Subject	Slow contraction		Moderate speed contraction	
	No. MUs	PNR	No. MUs	PNR
S1	7.0 ± 0.0	35 ± 4	11.0 ± 0.0	42 ± 9
S2	8.0 ± 0.0	35 ± 4	10.5 ± 0.7	36 ± 4
S3	10.0 ± 0.0	37 ± 3	13 ± 1.4	35 ± 3
S4	9.0 ± 1.4	33 ± 2	9.5 ± 0.7	36 ± 4
S5	8.5 ± 0.7	35 ± 3	7.0 ± 1.7	35 ± 3
AVG.	**8.7 ± 1.1**	**35 ± 3**	**10.1 ± 2.3**	**36 ± 4**

hdEMG signals were recorded during moderate speed and slow extensions and flexions of knee joint. The results are averaged over two trials, except in S1 subject where only one trial was acquired.

TABLE II
Number and PNR of MUs, Identified From Rectus Femoris Muscle

Subject	Slow contraction		Moderate speed contraction	
	No. MUs	PNR	No. MUs	PNR
S1	7.0 ± 0.0	32 ± 2	10.0 ± 0.0	36 ± 5
S2	8.0 ± 0.0	33 ± 3	9.0 ± 0.0	38 ± 4
S3	8.0 ± 0.0	35 ± 2	7.0 ± 2.8	34 ± 2
S4	7.0 ± 0.0	33 ± 2	7.0 ± 0.0	35 ± 2
S5	8.5 ± 3.5	33 ± 2	7.5 ± 0.7	34 ± 3
AVG.	**7.8 ± 1.4**	**33 ± 2**	**7.9 ± 1.5**	**35 ± 3**

hdEMG signals were recorded during moderate speed and slow extensions and flexions of knee joint. The results are averaged over two trials, except in S1 subject where only one trial was acquired.

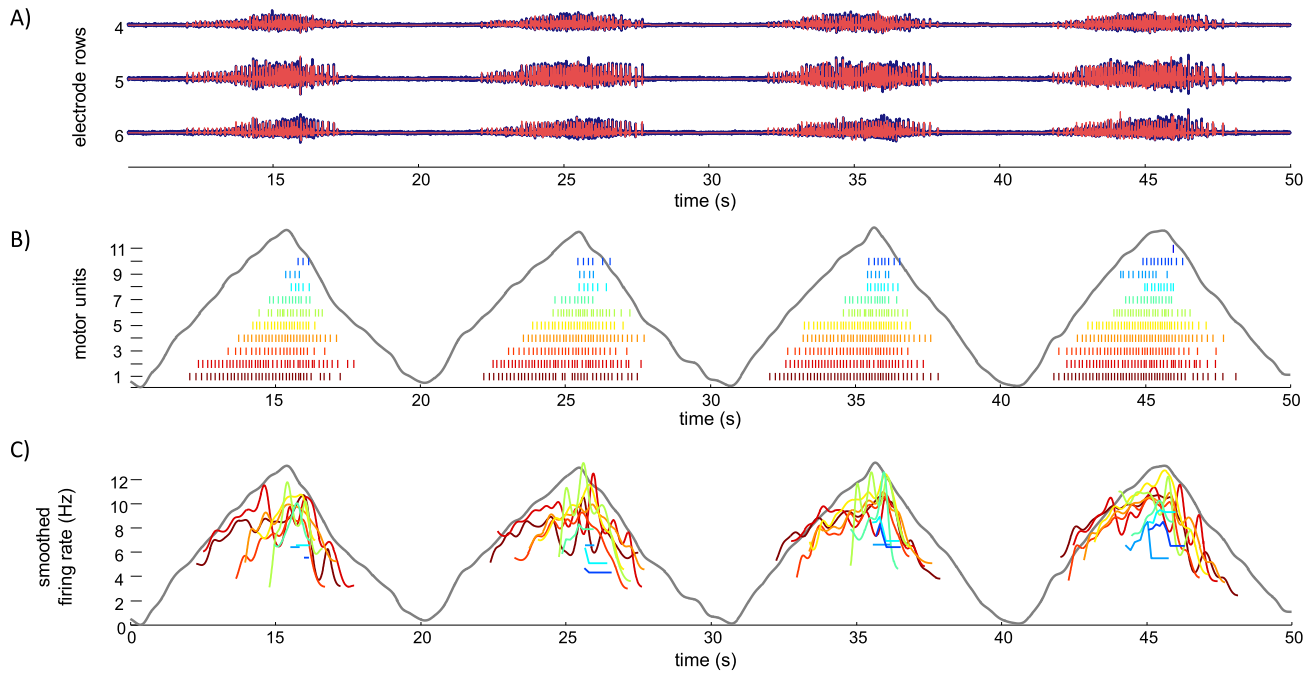

Fig. 8. Panel A depicts representative hdEMG signals (blue) and sum of identified MUAPs (red) from vastus lateralis muscle during dynamic knee extension and flexion. Panel B depicts the results of hdEMG decomposition into individual MU spike trains. Each vertical bar depicts one MU firing. Panel C depicts smoothed firing rate of identified MUs. Different MUs are depicted by different colors. Knee joint angle is depicted by solid grey line. For clarity reasons, only 4 out of 8 recorded contraction ramps are depicted.

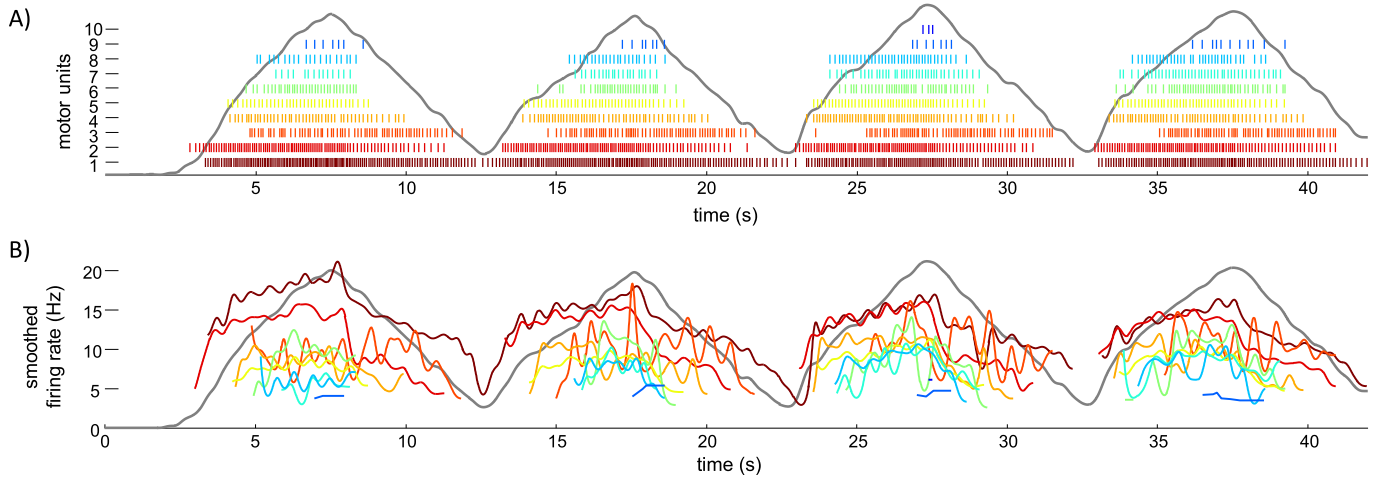

Fig. 9. Individual MU spike trains identified from rectus femoris muscle during dynamic knee extension and flexion (Panel A) and their smoothed firing rates (Panel B). Different MUs are depicted by different colors, whereas knee joint angle is depicted by solid grey line. For clarity reasons, only 4 out of 8 recorded ramps are depicted.

regardless the tested level of muscle excitation. The same applies to the sensitivity, precision and false alarm rate (Fig. 5). The number of accurately identified MUs was relatively high and comparable to the results of isometric decomposition. This also depends on the number of decomposition runs as up to one MU is identified by cyclostationary CKC in each decomposition run. In this study, the number of decomposition runs was limited to 100, based on our experiences in isometric conditions [12]–[17].

The results on synthetic hdEMG signals also show that the PNR $\geq$ 30 dB, introduced in isometric conditions [18], corresponds to high sensitivity and precision (>90 %) and low false alarm rate (<1 %) in identification of MU firings also in dynamic conditions (Fig. 6). This threshold value is likely conservative in dynamic conditions as we clearly demonstrated that the PNR value is also affected by the changes of MUAPs during muscle shortening. Thus, the criterion of PNR $\geq$ 30 dB should be used for local PNR, whereas considerably lower global PNR values were frequently observed in MUs with sensitivity >90 % (Fig. 6).

The experimentally estimated MUAPs during the dynamic contraction of biceps brachii muscle showed relatively large range of MUAP changes. The average correlation coefficient between the MUAPs at the muscle fully extended and the

muscle fully shortened was 0.47 ± 0.3 (Fig. 2). This number was assessed over 252 experimentally identified MUs and the accuracy of MU identification was indirectly confirmed by the continuity of the MUAP shapes (Fig. 2) and by the very strict selection criteria (global PNR $>$ 30 dB and manual inspection of each identified MU spike train). The presented changes of MUAP shapes may, thus, be considered representative for the short head of biceps brachii in young healthy subjects.

The results of experimental decomposition of hdEMG signals in vastus lateralis and rectus femoris muscle agree with the ones from synthetic hdEMG signals. The number of identified MUs was lower than in the synthetic case, but this is reasonable given the relatively low level of muscle contraction force.

The processing time required by newly proposed cyclostationary CKC method depends on the sensitivity of identified MUs to the exerted geometric changes of the investigated muscle. In our tests, the method required $\sim$20 minutes on Intel i7 processor with 32 GB of memory to decompose 60 s long hdEMG signals. For comparison, classical CKC method requires around 9 minutes for decomposition of 60 s long isometric hdEMG signals.

For the purpose of fair comparison, the length of hdEMG signals has been kept constant in this study, regardless the speed of muscle contraction. Clearly, several repetitions of the same muscle movement are required by the decomposition concepts presented herein. The sensitivity of MU identification to the number of movement repetitions per trail is muscle and contraction level specific and its detailed analysis exceeds the scope of this study. As a general rule, the higher the speed of movement, the larger the required number of movement repetitions. Noteworthy, the movement repetitions do not need to be of the same duration as the MU tracking implemented in Step 6 of Pseudocode 1 automatically determines the optimal time support for MU spike identification in each movement repetition.

Finally, no attempt has been made to keep the contraction levels of vastus lateralis and rectus femoris strictly constant during their shortening. Therefore, the presented MU firing patterns reflect the natural MU control strategies during the dynamic knee flexion and extension. No attempt has been made to explain the differences in the MU firing rates during concentric and eccentric phase and also to explain the differences between the firing pattern of MUs in vastus lateralis and rectus femoris muscle. These explanations would require much larger number of repeated muscle contractions and are beyond the scope of this study.

In conclusion, we have introduced the new methodology that extends the previously presented CKC decomposition technique to repeated dynamic contractions. The introduced methodology demonstrated considerable robustness to MUAP changes and speed of muscle contraction. Therefore, it has a substantial potential in studies of human movement, at least in controlled environments. Further studies are required to assess the appropriateness of the described methodology for MU identification in different skeletal muscles and to analyze its sensitivity to the number of muscle contraction repetitions.

REFERENCES

[1] J. H. Blok, J. P. van Dijk, G. Drost, M. J. Zwarts, and D. F. Stegeman, "A high-density multichannel surface electromyography system for the characterization of single motor units," *Rev. Sci. Instrum.*, vol. 73, no. 4, p. 1887, 2002.

[2] M. Chen, A. Holobar, X. Zhang, and P. Zhou, "Progressive FastICA peel-off and convolution kernel compensation demonstrate high agreement for high density surface EMG decomposition," *Neural Plasticity*, vol. 2016, Aug. 2016, Art. no. 3489540.

[3] M. Chen and P. Zhou, "A novel framework based on FastICA for high density surface EMG decomposition," *IEEE Trans. Neural Syst. Rehabil. Eng.*, vol. 24, no. 1, pp. 117–127, Jan. 2016.

[4] D. Farina *et al.*, "The extraction of neural information from the surface EMG for the control of upper-limb prostheses: Emerging avenues and challenges," *IEEE Trans. Neural Syst. Rehabil. Eng.*, vol. 22, no. 4, pp. 797–809, Jul. 2014.

[5] D. Farina and A. Holobar, "Human? Machine interfacing by decoding the surface electromyogram [life sciences]," *IEEE Signal Process. Mag.*, vol. 32, no. 1, pp. 115–120, Jan. 2015.

[6] D. Farina and A. Holobar, "Characterization of human motor units from surface EMG decomposition," *Proc. IEEE*, vol. 104, no. 2, pp. 353–373, Feb. 2016.

[7] A. J. Fuglevand, D. A. Winter, and A. E. Patla, "Models of recruitment and rate coding organization in motor-unit pools," *J. Neurophysiol.*, vol. 70, pp. 2470–2488, Dec. 1993.

[8] J. A. Gallego *et al.*, "Influence of common synaptic input to motor neurons on the neural drive to muscle in essential tremor," *J. Neurophysiol.*, vol. 113, no. 1, pp. 182–191, 2014.

[9] J. A. Gallego *et al.*, "The phase difference between neural drives to antagonist muscles in essential tremor is associated with the relative strength of supraspinal and afferent input," *J. Neurosci.*, vol. 35, no. 23, pp. 8925–8937, 2015.

[10] V. Glaser, D. Farina, and A. Holobar, "Simulations of high-density surface electromyograms in dynamic muscle contractions," in *Proc. 39th Annu. Int. Conf. IEEE Eng. Med. Biol. Soc.*, Seogwipo, South Korea, Jul. 2017, pp. 3453–3456.

[11] E. Henneman, "Relation between size of neurons and their susceptibility to discharge," *Science*, vol. 126, pp. 1345–1347, Dec. 1957.

[12] A. Holobar and D. Zazula, "Correlation-based decomposition of surface electromyograms at low contraction forces," *Med. Biol. Eng. Comput.*, vol. 42, no. 4, pp. 487–495, 2004.

[13] A. Holobar and D. Zazula, "Multichannel blind source separation using convolution kernel compensation," *IEEE Trans. Signal Process.*, vol. 55, no. 9, pp. 4487–4496, Sep. 2007.

[14] A. Holobar, D. Farina, M. Gazzoni, R. Merletti, and D. Zazula, "Estimating motor unit discharge patterns from high-density surface electromyogram," *Clin. Neurophysiol.*, vol. 120, no. 3, pp. 551–562, 2009.

[15] A. Holobar, M. A. Minetto, A. Botter, F. Negro, and D. Farina, "Experimental analysis of accuracy in the identification of motor unit spike trains from high-density surface EMG," *IEEE Trans. Neural Syst. Rehabil. Eng.*, vol. 18, no. 3, pp. 221–229, Jun. 2010.

[16] A. Holobar, V. Glaser, J. A. Gallego, J. L. Dideriksen, and D. Farina, "Non-invasive characterization of motor unit behaviour in pathological tremor," *J. Neural Eng.*, vol. 9, no. 5, p. 056011, 2012.

[17] A. Holobar and D. Farina, "Blind source identification from the multichannel surface electromyogram," *Physiol. Meas.*, vol. 35, no. 7, pp. R143–R165, 2014.

[18] A. Holobar, M. A. Minetto, and D. Farina, "Accurate identification of motor unit discharge patterns from high-density surface EMG and validation with a novel signal-based performance metric," *J. Neural Eng.*, vol. 11, no. 1, p. 016008, 2014.

[19] T. Kapelner *et al.*, "Motor unit characteristics after targeted muscle reinnervation," *PLoS ONE*, vol. 11, no. 2, p. e0149772, 2016.

[20] X. Li, A. Holobar, M. Gazzoni, R. Merletti, W. Z. Rymer, and P. Zhou, "Examination of poststroke alteration in motor unit firing behavior using high-density surface EMG decomposition," *IEEE Trans. Biomed. Eng.*, vol. 62, no. 5, pp. 1242–1252, May 2015.

[21] H. R. Marateb, K. C. McGill, A. Holobar, Z. C. Lateva, M. Mansourian, and R. Merletti, "Accuracy assessment of CKC high-density surface EMG decomposition in biceps femoris muscle," *J. Neural Eng.*, vol. 8, no. 6, p. 066002, 2011.

[22] R. Merletti and D. Farina, *Surface Electromyography: Physiology, Engineering, and Applications* (IEEE Series Biomedical Engineering). Hoboken, NJ, USA: Wiley, 2016.

[23] M. Mordhorst, T. Heidlauf, and O. Röhrle, "Predicting electromyographic signals under realistic conditions using a multiscale chemo–electro–mechanical finite element model," *Interface Focus*, vol. 5, no. 2, p. 20140076, 2015, doi: 10.1098/rsfs.2014.0076.

[24] S. Muceli *et al.*, "Accurate and representative decoding of the neural drive to muscles in humans with multi-channel intramuscular thin-film electrodes," *J. Physiol.*, vol. 593, no. 17, pp. 3789–3804, 2015.

[25] S. H. Nawab, S. S. Chang, and C. J. De Luca, "High-yield decomposition of surface EMG signals," *Clin. Neurophysiol.*, vol. 121, no. 10, pp. 1602–1615, 2010.

[26] F. Negro and D. Farina, "Linear transmission of cortical oscillations to the neural drive to muscles is mediated by common projections to populations of motoneurons in humans," *J. Physiol.*, vol. 589, no. 3, pp. 629–637, 2011.

[27] F. Negro, S. Muceli, A. M. Castronovo, A. M. Holobar, and D. Farina, "Multi-channel intramuscular and surface EMG decomposition by convolutive blind source separation," *J. Neural Eng.*, vol. 13, no. 2, p. 026027, 2016.

[28] Y. Ning, X. Zhu, S. Zhu, and Y. Zhang, "Surface EMG decomposition based on K-means clustering and convolution kernel compensation," *IEEE J. Biomed. Health Inf.*, vol. 19, no. 2, pp. 471–477, Mar. 2015.

[29] P. P. Bržan *et al.*, "New perspectives for computer-aided discrimination of parkinson's disease and essential tremor," *Complexity*, vol. 2017, Oct. 2017, Art. no. 4327175.

[30] J. Roussel, P. Ravier, M. Haritopoulos, D. Farina, and O. Buttelli, "Decomposition of multi-channel intramuscular EMG signals by cyclostationary-based blind source separation," *IEEE Trans Neural Syst. Rehabil Eng.*, vol. 25, no. 11, pp. 2035–2045, Nov. 2017.

[31] K. Watanabe, A. Holobar, M. Kouzaki, M. Ogawa, H. Akima, and T. Moritani, "Age-related changes in motor unit firing pattern of vastus lateralis muscle during low-moderate contraction," *AGE*, vol. 38, no. 3, p. 48, 2016.

[32] U. Ş. Yavuz *et al.*, "Estimating reflex responses in large populations of motor units by decomposition of the high-density surface electromyogram," *J. Physiol.*, vol. 593, no. 19, pp. 4305–4318, 2015.